CHEMISTRY OF MATERIALS

pubs.acs.org/cm

Article

Solution Atomic Layer Deposition of Smooth, Continuous, Crystalline Metal−Organic Framework Thin Films

Maïssa K. S. Barr,* Soheila Nadiri, Dong-Hui Chen, Peter G. Weidler, Sebastian Bochmann, Helmut Baumgart, Julien Bachmann, and Engelbert Redel*

Cite This: *Chem. Mater.* 2022, 34, 9836−9843

Read Online

ACCESS | Metrics & More | Article Recommendations | Supporting Information

ABSTRACT: For the first time, a procedure has been established for the growth of surface-anchored metal−organic framework (SURMOF) copper-(II) benzene-1,4-dicarboxylate (Cu-BDC) thin films of thickness control with single molecule accuracy. For this, we exploit the novel method solution atomic layer deposition (sALD). The sALD growth rate has been determined at 4.5 Å per cycle. The compact and dense SURMOF films grown at room temperature by sALD possess a vastly superior film thickness uniformity than those deposited by conventional solution-based techniques, such as dipping and spraying while featuring clear crystallinity from 100 nm thickness. The highly controlled layer-by-layer growth mechanism of sALD proves crucial to prevent unwanted side reactions such as Ostwald ripening or detrimental island growth, ensuring continuous Cu-BDC film coverage. This successful demonstration of sALD-grown compact continuous Cu-BDC SURMOF films is a paradigm change and provides a key advancement enabling a multitude of applications that require continuous and ultrathin coatings while maintaining tight film thickness specifications, which were previously unattainable with conventional solution-based growth methods.

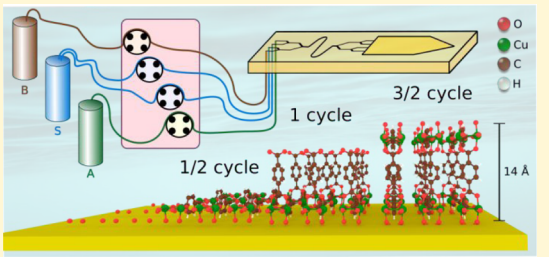

INTRODUCTION

Metal−organic frameworks (MOFs)[1−3] can be described as crystalline three-dimensional microporous solids featuring a high surface area. They have attracted considerable attention in a wide range of applications, for example, in catalysis,[4] hydrogen storage,[5,6] gas separation,[7] thermoelectric applications,[8−10] or as chemical sensors.[11] For these applications, open coordination sites at the metal center have been demonstrated to play a crucial role.[12,13] Cu-BDC is constructed of multiple Cu paddlewheel units coordinating four 1,4-benzenedicarboxylate linkers, as shown schematically in Figure 1.[14,15] Cu-BDC is one of the most known, common, and interesting MOF materials as it can be prepared from common, commercially available, and inexpensive commodity chemicals.

Standard atomic layer deposition (ALD) is a gas-phase thin-film deposition technique based on a sequential repetition of complementary, self-limiting reactions between volatilized molecular precursors and the solid sample surface. ALD facilitates the deposition of ultrathin films with reliable accuracy in terms of superior film thickness control at the Angstrom (Å) scale to meet the demands of the current nanotechnology, due to the strict control of the process by self-limiting gas surface reactions, enabling conformal surface coverage of device geometries with very high aspect ratios. Conventional gas-phase ALD is characterized by its cyclic operational mode in which a binary film is being synthesized by the sequential self-limited reactions between volatilized precursor and co-reactant vapors that are introduced into the reactor chamber in an alternating manner and separated by intermediate inert gas purges, thereby saturating every sample and reactor surface. Conventional ALD performed with gaseous precursors (thermally or plasma-enhanced) has become an accepted high-volume industrial technology with worldwide importance in the fields of microelectronics, electroluminescent display, and photovoltaics, specifically for the synthesis of high-k dielectric films and metal gates in MOSFET gate stacks, as dielectric layers of DRAM capacitors or as passivating layers.[16−18] ALD procedures and reactors are well established for the deposition of oxides, sulfides, nitrides, selenides, tellurides, and elemental noble metals.[19] However, important classes of thin-film materials are not accessible by conventional ALD from gaseous precursors, prominent examples being organic materials (e.g., polymers), hydrides, and ionic solids. Hybrid (metal−organic) materials have been accessed by gas-phase ALD as the so-called "molecular layer deposition" (MLD) generalization; however, the range of compounds accessible in MLD is quite narrow.[20−23] This is related to the limited choice of molecular precursors that

Received: April 11, 2022
Revised: September 14, 2022
Published: November 2, 2022

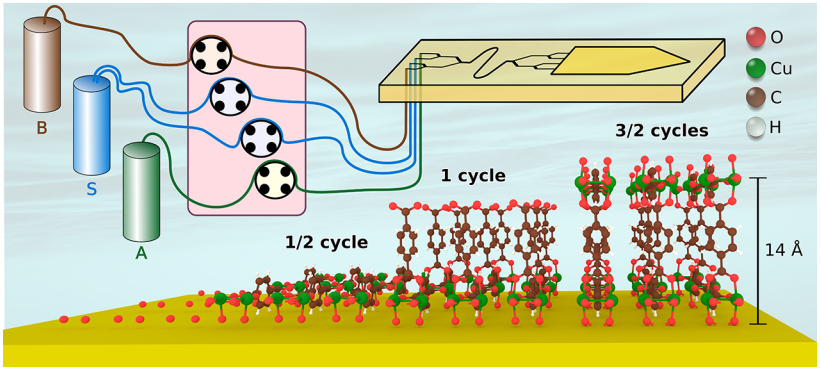

Figure 1. Scheme of the sALD setup outlining the peristaltic pump arrangement with the connections to the reaction chamber and the growth of Cu-BDC. A corresponds to the first precursor path ($Cu_2(OAc)_4$), B to the second precursor path (terephthalic acid), and S to the solvent path (ethanol). Furthermore, the size of the Cu-BDC unit cell of 14 Å is indicated.

possess sufficient thermal stability and volatility.[24,25] ZIF-8 MOF has been obtained from a conversion of ALD-grown ZnO.[26] Success in the direct growth of MOFs by ALD has remained limited.[27−30] In the literature, it is reported that the crystallinity is obtained upon post-deposition processing, either with a thermal annealing step or an extended aging at room temperature. Gas-phase deposition methods usually compete with the limited thermal stability of MOFs. However, MOF-CVD processes have been established by the group of Rob Amelot.[26,31−33]

Performing self-limited surface reactions from dissolved precursors instead of gaseous ones in "solution ALD" (sALD) broadens the range of usable precursors significantly.[34−36] The broader range of precursors, combined with the presence of solvent (at atmospheric pressure) and the low deposition temperatures, renders sALD particularly attractive for novel families of solids, in particular MOFs. So far, MOF syntheses have always relied on solution-based processing. Beyond classical solvothermal approaches for the synthesis of bulk powder, growth techniques for thin-film MOFs, or SURMOFs, rely on a volatile organic solvent which precipitates the solid upon evaporating: spin-coating, spray-coating, dip-coating, immersion, and pump methods. These traditional methods generate MOF thin films with a rather low film quality and are further handicapped by a severe lack of film thickness control, which renders them unsuitable for most applications and for all practical purposes that exclude any industrial device prospects. We note that the spray-coating method has also been presented under the phrases "liquid-phase epitaxy" (LPE) and "layer-by-layer" deposition,[37−40] which suggest a degree of relatedness higher than it may seem at first. Indeed, even if two precursors are sprayed onto the substrate sequentially (in analogy to ALD), two major differences result in a distinct growth mechanism. The facts that first, the solutions are significantly more concentrated, and second, after each step the solutions are left to dry (at least partially), concur to cause the precipitation of the solid. Therefore, in spray-coating (a.k.a. "liquid-phase epitaxy" and "layer-by-layer" deposition), the amount deposited is not controlled by surface chemistry. Correspondingly, the morphology of the deposit is far from perfection (as we will see later).

Here, we demonstrate for the first time that exploiting the sALD principles for MOF thin-film growth results in superior film quality with previously unmatched precise film thickness control at the molecular level. With sALD of Cu-BDC SURMOF, no unwanted thin-film growth mechanism has been observed such as Ostwald ripening,[41] island growth,[42] and inhomogeneous film formation.[42]

Such thin and continuous films are ideal for gas sensing applications, for instance, in which the electrical conductivity of the MOF layer is affected by condensation and/or coordination of organic analyte vapors in the open porous structure.[43] Previous MOF synthesis methods have relied on either discontinuous MOF phases (in the form of powders or islands on substrates) or their thick films. Neither of those situations is ideal for gas sensing, either due to the limited contact between the solid and the gas phase or due to the lack of homogeneous conduction across the sample, or even a combination of both. The system that we present here combines all advantageous features needed for such an application.

Experimental Methods. *Substrate Preparation.* Prior to deposition, Si wafer pieces of 1 × 1 to 1 × 2 cm^2 size were cleaned with an oxygen plasma for 30 min, which leaves the native oxide intact. All Cu-BDC SURMOF layers were grown using sALD in a microfluidic reactor sketched in Figure 1 on nonfunctionalized Si wafers (featuring the usual amorphous native oxide SiO_2), except for those dedicated to IRRAS and Raman analyses, which were grown on Au-covered Si substrates functionalized with a SAM (self-assembled monolayer) of 16-mercaptohexadecanoic acid (MHDA, 99%, Aldrich). These two types of substrates were selected as they represent the most used ones in the literature for investigating the growth of Cu-BDC with conventional solution processes.

Synthesis of Cu-BDC SURMOF Films by sALD. The deposition of Cu-BDC was carried out in a custom-built microfluidic reactor equipped with peristaltic original equipment manufacturer pumps, as described earlier by Wu,[36] Fichtner,[34] and Koch (Figure 1), and further details are provided in the Supporting Information[35] The sALD controller and software were provided by ZUMOlab. The microfluidic reactor is made out of Teflon, where four inlets supply the precursors and solvent to the sALD reactor chamber. The first (pump A) and the fourth (pump B) inlets are dedicated to delivering the two required precursors, while the second (pump S) and the third (pump S) inlets are dedicated to supplying the purge solvent.

Dicopper(II) tetraacetate ($Cu_2(OAc)_4$) and benzene-1,4-dicarboxylic acid (BDC, terephthalic acid) are used as the precursors for the copper source and the linker, respectively, while ethanol is the solvent. Both precursors are diluted in absolute ethanol (0.6 and 2 mM for copper acetate and BDC,

https://doi.org/10.1021/acs.chemmater.2c01102
Chem. Mater. 2022, 34, 9836−9843

respectively). Cu-BDC sALD proceeds by repeating the following deposition cycle: injection of the first precursor (Cu acetate, 30 s) into the reaction chamber is followed by a static exposure (30 s) and a subsequent purge with pure solvent (90 s). The sALD cycle is completed by the subsequent injection of the second precursor (benzene-1,4-dicarboxylic acid), followed by exposure and purge, using the same duration as for the first precursor. This sALD cycle is performed N times in total ($10 \leq N \leq 400$) to attain a variety of SURMOF film thicknesses. Beyond these standard parameters, successful ALD growth is demonstrated by characterizing the influence of the critical process parameters. The effect of purge duration was studied using the following ALD pulse/exposure/purge sequences: 30 s/30 s/x s (x = 30, 60, 90, 120, 150, 175). Similarly, the effect of pulse duration was investigated with the sequences y s/30 s/90 s (y = 5, 10, 20, 30, 50), and the pulse duration of both precursors was varied simultaneously. The sALD procedure closes with the solvent purge of the last cycle, after which the microfluidic chamber is open and the sample air-dried. As a comparison for benchmarking, Cu-BDC was deposited by spray-coating and dip-coating. In order to compare different deposition methods while maintaining the same chemical reactions, we grow Cu-BDC by sALD using the same precursors and solvent established in LPE and dip-coating. For the samples used in IRRAS and Raman measurements, all Cu-BDC SURMOFs used in the present work were grown on modified Au-covered substrates using the LPE method.[38] The surface modification of gold-covered substrates was carried out by depositing a SAM made from 16-mercaptohexadecanoic acid (MHDA, 99%, Aldrich). The SURMOFs were fabricated using the LPE spray method, as described in detail in previous publication.[39]

The spray times were 15 s for the $Cu_2(OAc)_4$ ethanolic solution and 25 s for the BDC ethanolic solution. Each spray step was followed by a rinsing step of 3−5 s with pure ethanol. A total of 20−150 growth cycles were used for the Cu-BDC SURMOFs investigated in this work.

The synthesis of Cu-BDC SURMOF thin films by dipping used the following procedure done by hand: Au substrates with functionalized MHDA SAMs or clean Si substrates are dipped into 1 mM $Cu_2(OAc)_4$ ethanolic solution for a duration of 30 min. After this, the sample is rinsed with ethanol. Next, the sample is placed into a 0.2 mM BDC ethanolic solution for 45 min. After this, the sample is rinsed again with ethanol.

The desired film thickness of Cu-BDC SURMOF thin films is generated through a repeated process of alternate immersion and rinsing, for example, 5, 10, 20, or 50 cycles.

Material Characterization. A SENPro spectroscopic ellipsometer from SENTECH was used to measure the resulting Cu-BDC SURMOF film thickness grown on Si substrates. All measurements were performed at a fixed angle of 70° in a spectral range of 370−1050 nm before and after sALD deposition. A Cauchy model is used to determine the thickness of Cu-BDC based on the article by Redel et al.[44] The liquid quartz crystal microbalance (QCM) cell model "openQCM" was purchased from Novaetech. AFM images were obtained with a Veeco Dimension 3100 microscope using tapping mode. Silicon probe tips from Bruker were used with a spring constant 2 N m^{-1} and resonance frequency 70 kHz. The resolution is 1024 × 1024 and 512 × 512 pixels for the imaged surfaces of either 2 × 2 or 20 × 20 μm^2, respectively. The digital image processing was performed with Gwyddion 2.53, and the root-mean-square (rms) roughness was determined with the statistical tool embedded in the software. Masking in Figure 5d−f was performed on topographic images using 3.2, 6.2, and 4.4 nm as the thresholds. The threshold values were chosen so as to fit visually with the phase images (a,b,c). The XRD measurements in out-of-plane (coplanar) orientation were collected on a Bruker D8-Advance diffractometer equipped with a position-sensitive detector Lynxeye in $\theta-\theta$ geometry, a variable divergence slit, and 2.3° Soller slit on the primary and secondary sides. The measurement was carried out in the range of 2θ = 4 to 47° at a scan step of 0.019° utilizing Cu Kα1,2 radiation (λ = 0.15406 nm) generated at 40 kV and 40 mA. For the samples prepared on Au-covered substrates, after background correction, the height correction was performed using the substrate diffraction peak positions Au(111), which were measured additionally at the end of each run. The infrared reflection−absorption spectra (IRRAS) of the samples in this study were acquired with a wavenumber resolution of 2 cm^{-1} using a Bruker VERTEX 80v spectrometer in grazing incidence reflection mode at an angle of incidence of 10°, using a liquid nitrogen-cooled HgTe−CdTe narrow-band detector. Perdeuterated hexadecanethiol SAMs on Au were used for reference measurements. Raman spectra were measured using a Bruker Senterra Raman microscope (Bruker Optics, Ettlingen, GER), equipped with a 50× Olympus MPLAN objective NA 0.45 and a frequency-doubled DPSS NdYAG-Laser, λ = 532 nm, operated at 200 μW output power. Each spectrum was measured with 180 s integration time using three co-additions (3 × 60 s). For data acquisition as well as spectra evaluation, the Bruker OPUS software v7.5 was used. The SEM measurements were performed on a Gemini 500, Carl Zeiss field-emission instrument.

RESULTS AND DISCUSSION

Solution ALD of Cu-BDC. The sALD growth rate of Cu-BDC SURMOF films was determined by spectroscopic ellipsometry (Figure 2a) on Si substrates with a native oxide pretreated by oxygen plasma. The evolution of the film thickness of Cu-BDC as a function of the number of

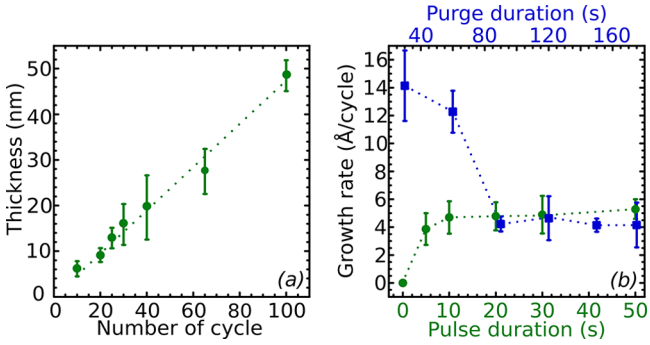

Figure 2. (a) Linear Evolution of the film thickness as a function of the number of sALD growth cycles for the sALD pulse/exposure/purge sequence of 30 s/30 s/90 s. (b) Saturation curve of the sALD growth rate as a function of the pulse and purge durations (green and blue, respectively). For the saturation study, the pulse duration of both precursors was varied simultaneously. The error bars show the uncertainty on the measurements. They correspond to the standard deviation averaged over at least 5 points measured by spectroscopic ellipsometry on a Si substrate with native oxide. The growth rate is 4.5 Å/ALD cycle.

https://doi.org/10.1021/acs.chemmater.2c01102
Chem. Mater. 2022, 34, 9836−9843

deposition cycles N is shown in Figure 2a for the sALD pulse/exposure/purge sequence 30 s/30 s/90 s. As expected for an ALD (or MLD) process, the thickness increases linearly with the number of ALD growth cycles (also visible from the quartz crystal microbalance data in Figure S1). The fitted linear curve intercepts the origin which indicates that there is no nucleation delay (Figure 2a). The sALD growth rate extracted from this plot is 4.5 Å/ALD cycle which corresponds exactly to one-third of a Cu-BDC unit cell, and a schematic of the growth is presented in Figure S2. This demonstrates that for one sALD deposition cycle, less than one complete monolayer is deposited mostly due to steric hindrance, which is common in ALD or MLD processes.[45] For comparison with one well-known ALD example, the growth of Al_2O_3 from a classic gas-phase ALD reaction also corresponds to one-third of a unit cell per cycle.[19,45] In order to confirm that the growth of Cu-BDC SURMOF films corresponds to an ALD or MLD process, it is crucial to produce evidence of the independence of the growth rate as a function of the variation of the precursor dosage. For this purpose, the pulse duration of both precursors was varied from 5 to 50 s, while the purge time was maintained at 90 s for each experiment. The evolution of the growth rate as a function of the pulse duration exhibits a plateau saturating after 10 s (Figure 2b). Pulses shorter than 10 s do not deliver sufficient precursor dosage to achieve surface saturation. This typical saturation behavior provides experimental proof of the self-limiting behavior of the surface chemistry characteristic of ALD (or MLD). In all the following experiments, a pulse duration of 30 s is adopted as the standard. An additional confirmation of self-limiting surface chemistry is provided by a purge duration variation (while the pulse is maintained constant at 30 s, Figure 2b). This experiment establishes that 90 s is the minimal purge duration needed to avoid the direct simultaneous contact and mixing between both precursors. In all following work, the purge time is kept constant at 90 s.

Material Characterization. The chemical composition is identified by PM-IRRAS and Raman, as shown in Figure 3a.

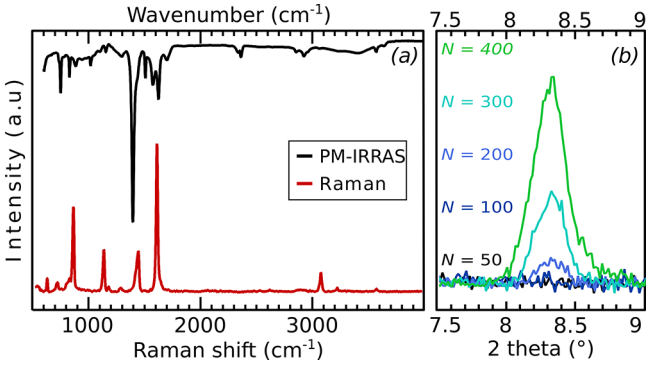

Figure 3. (a) PM-IRRAS and Raman spectra of Cu-BDC grown by sALD with 50 ALD cycles and (b) XRD diffractogram of Cu-BDC grown by sALD with 50, 100, 200, 300, and 400 ALD cycles.

The IRRAS peaks at 2931 and 753 cm^{-1} wavenumbers correspond to aromatic C−H stretching and bending vibrations, respectively[46−48] Additionally, the presence of the linker is confirmed with the detection of the stretching C═C from the aromatic ring, with the emergence of the peaks at 1571 and 1507 cm^{-1}, while the peak at 1690 cm^{-1} originated from the C═O group from carbonyl.[46−48] However, the coordination of the linker to the metal ion is proved by the presence of the peaks at 1629 and 1397 cm^{-1} which correspond to asymmetric and symmetric stretching vibrations of the ——COO^- group, respectively.[49,50] No broad peaks can be detected around 3400 and 2900 cm^{-1}. Within the limited informative value of this observation given the low signal associated with the thin film, this seems to indicate that neither water nor ethanol has been trapped in the SURMOF pores.[48] The Raman spectra also provide another independent confirmation of the presence of the linker. The Raman peaks at 3077, 1641, and 1441 cm^{-1} are attributed to C−H, C═C, and C−O, respectively.[48,49] Additionally, the presence of the BDC ring is clarified with the presence of the peak at 1140 cm^{-1}.[48,49] The chemical composition does not vary with the increase of the thickness. The PM-IRRAS and Raman spectra are identical for 50 and 200 sALD cycles (Figure S3). The crystalline structure of Cu-BDC grown by sALD has been identified by X-ray diffraction in Cu-BDC films grown with 50, 100, 200, 300, and 400 ALD deposition cycles, as depicted in Figure 3b. The sole XRD reflection at $2\theta = 8.3°$ can be indexed to the presence of crystalline Cu-BDC and is the only one detected over the range between 0° and 30°; the full diffractogram is shown in Figure S4, and the peak detected at 23° is attributed to the sample holder.[32] However, for ALD deposition cycles less than 200 cycles, no XRD peak can be observed neither in Bragg−Brentano geometry nor in grazing incidence geometry due to the extremely low thickness of the SURMOF layer resulting in insufficient information volume. This indicates that the film most likely starts out in amorphous phase or mixed amorphous phase with embedded nanocrystallites or insufficient information volume in the thin film for XRD to pick up any crystal reflection signal from the onset of crystalline nucleation. Then, it crystallizes once the Cu-BDC film exceeds a critical thickness of about 100 nm which could correspond to the formation of an extended lattice providing sufficient driving force for crystallization or when there is sufficient information volume in the sample to detect the single growth revealed by the single XRD reflection at 8.3°. From 200 to 400 cycles, the intensity of XRD reflection increases with the number of ALD cycles, and this provides the experimental evidence of an oriented crystalline state of Cu-BDC, which is a necessary requirement for a SURMOF film. For the sample with 400 cycles, a second order peak (200) was observed. As no other peaks were detected, a preferred orientation along the [100] direction must be concluded. Our work is the first study, which demonstrates the growth of crystalline Cu-BDC film at room temperature with an ALD/MLD process without thermal treatment.

The surface morphology and the roughness of Cu-BDC SURMOF films deposited by sALD have been characterized by SEM and AFM (Figure 4). The SEM micrograph of a Cu-BDC film after 10 sALD cycles is presented in Figure 4a. The relatively featureless image is consistent with a compact, dense, and continuous film, in stark contrast to the typical prevailing morphology of Cu-BDC deposited by conventional methods of spray-coating or dip-coating, which consists mostly of nanosheets, needles, or large particles.[32,47,51,52] The homogeneity is retained for larger numbers of cycles (Figure S5). A cross-sectional micrograph and an EDX spectrum which confirm the compactness of the layer and the presence of Cu-BDC are shown in Figure S6. The Cu-BDC SURMOF film continuity and morphological quality are further proven by AFM analysis. The AFM topographic micrographs reveal small grainy features homogeneously distributed over the film, in a

https://doi.org/10.1021/acs.chemmater.2c01102
Chem. Mater. 2022, 34, 9836−9843

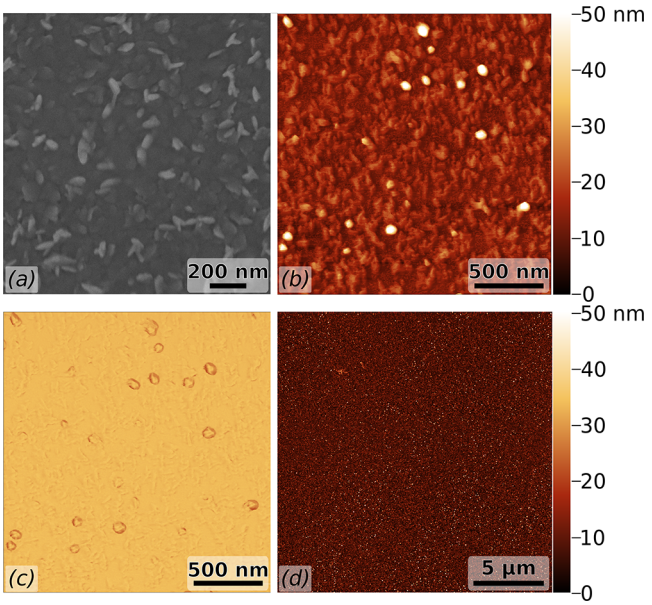

Figure 4. Microscopic characterization of Cu-BDC films grown with 10 sALD cycles. (a) SEM micrograph of surface morphology and (b) AFM micrograph of Cu-BDC film grown with 10 deposition cycles by sALD. (c) Phase contrast data of the AFM micrograph (scale −75 to 75°). (d) Low-magnification AFM micrograph of the same film. Micrographs (b) and (c) display the same area of the film, which differs from those shown in (a) and (d). The rms roughness obtained from image (d) is 5.1 nm.

manner similar to the SEM display (Figure 4b,d). The phase contrast image confirms that the Cu-BDC film coverage is already continuous after 10 sALD growth cycles (Figure 4c).

For benchmarking, a direct comparison of sALD SURMOF films is provided with films deposited with similar thickness (4.5 nm) by the other conventional methods seen in the micrographs in Figure 5. The low nominal film thickness was chosen so as to emphasize the critical differences pertaining to film continuity most clearly (given that most films will eventually evolve into continuous layers beyond a certain thickness). Here, the AFM phase contrast images (a,b,c) exhibit a very different pattern for the sALD case (a) versus the two conventional deposition methods of dip-coating and spray-coating (b,c): in these latter two cases, the AFM micrographs reveal discontinuous Cu-BDC films of clearly separate islands interrupted by large areas which are perfectly smooth, corresponding to the empty SiO_2 substrate surface, indicating the missing Cu-BDC film, whereas in the sALD case (a), the resulting Cu-BDC film is completely continuous with homogeneous surface coverage. Taking these smooth areas as the empty native SiO_2 substrate surface with no discernible Cu-BDC film, we apply a threshold mask to the topographic images (d,e,f) in order to highlight the areas left noncovered by dip-coating and spray-coating, also called "liquid-phase epitaxy" or "layer-by-layer" deposition.[37−40] Clearly, the sALD method achieves the crucially important homogeneous nucleation and growth completely covering the entire sample surface, whereas the less-controlled conventional methods yield only localized nucleation and formation of isolated islands with a lot of empty space in between characterized by the missing film. Importantly, this statement remains valid even for the spray-coating method, which also features sequential delivery of two distinct precursor solutions but without the self-limiting surface chemical nature of ALD.[38−41] The improvement in the achieved performance of the sALD thin-film growth is best illustrated in a direct comparison of how much surface area film coverage can be achieved by each method, which measures the percentage of continuous film coverage of the sample surface. In the sALD case, the covered area by the SURMOF film represents 99.6% of the entire sample surface (based on the 25 μm^2 shown) but only 33.1 and 28.2% for the other two conventional growth methods of dip-coating and spray-coating. This discontinuous island

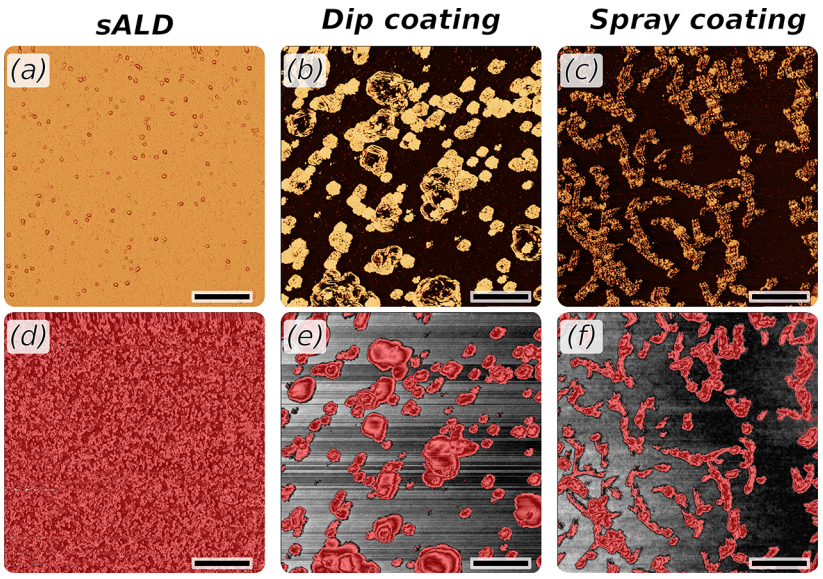

Figure 5. (a,d) AFM micrographs of Cu-BDC deposited by sALD with 10 deposition cycles, (b,e) dip-coating, and (c,f) spray-coating (a. k. a. "liquid-phase epitaxy" and "layer-by-layer" deposition). The micrographs (a−c) represent the phase contrast (the value varies between 0 and 70°) and (d−f) are the respective topographic data with a threshold mask, the height scale varying from 0 to 50 nm for (d,e) and from 0 to 25 nm for (f). The corresponding mask appears in red, and the unmasked region appears in black and white. The details of masking are described in the Experimental Methods section. The lateral scale bar represents 250 nm.

https://doi.org/10.1021/acs.chemmater.2c01102
Chem. Mater. 2022, 34, 9836−9843

growth mechanism (also known as the Volmer−Weber thin-film growth characterized by heterogeneous nucleation), as well as Ostwald ripening, is typically reported for MOFs grown by conventional methods and constitutes a fundamental limitation for dip-coating and spray-coating.[36] It is precisely the lack of homogeneous nucleation combined with self-limiting surface-saturating chemical precursor reactions, which is intrinsic to sALD, that relegates dip-coating and spray-coating to the vastly inferior Cu-BDC film quality. A further advantage of the sALD method is the excellent adhesion that it confers on the film (Figure S7).

Thus, our experimental results demonstrate a crucial advantage of sALD and establish it as the method of choice for depositing ultrathin (<10 nm), homogeneous, compact, and continuous crystalline Cu-BDC SURMOF layers. This paradigm-changing breakthrough opens up SURMOF film technology to entirely new application fields. The compelling advantages of surface saturation in absolutely conformal thin-film coatings with subnanometer precision that propelled classical gas-phase ALD technology to the leading edge in microelectronics have now been transferred to solution-processed material systems such as MOFs. We expect that this fruitful combination will open up many opportunities in areas such as sensing, optical coatings, and printed electronics and launch renewed interest to extend the sALD method beyond MOFs to organic materials (e.g., polymers), hydrides, and ionic solids.

CONCLUSIONS

A solution atomic layer deposition (sALD) process has been established for the direct deposition of SURMOF (surface-anchored metal−organic framework) Cu-BDC as thin compact continuous films in crystalline, oriented form at room temperature. The use of sALD is unprecedented in the field of MOFs and SURMOFs and is key to controlling growth down to the atomic or molecular resolution. With respect to the more broadly established gas-phase ALD, sALD provides the ability to handle nonvolatile precursor components and requires specially designed yet simple microfluidic reactors to enable true ALD self-limiting surface-saturating chemical precursor reactions in solution. The fact that SURMOF films grown by sALD exhibit a perfect film continuity even for thicknesses below 10 nm with Angstrom thickness control represents a paradigm change, in contrast to the discontinuous islands obtained by the Volmer−Weber growth mechanism which limits the achievable film quality of the conventional SURMOF dip-coating and spray-coating methods of Cu-BDC. The growth rate of 4.5 Å per sALD cycle defines the thickness resolution achievable, which corresponds to one-third of the unit cell.

This places sALD centrally on the MOF technology map. In the near future, the compelling and inevitable generalization of the Cu-BDC sALD reaction demonstrated here to other MOF compounds and its expansion to large-area coatings will most certainly enable practical applications of various SURMOF films, with gas sensors as one prominent example. Furthermore, the unique ability of sALD to conformally coat nonplanar, macroporous substrates represents an attractive tool to enhance the performance of many devices via tuning the surface-to-volume ratio of the functional material. This sALD breakthrough for Cu-BDC SURMOF thin films opens up a novel approach to synthesizing SURMOF films that are in compliance with the most stringent thin-film specification requirements in the nanotechnology area and thus will potentially lead to new SURMOF device applications not yet foreseen.

ASSOCIATED CONTENT

Supporting Information

The Supporting Information is available free of charge at https://pubs.acs.org/doi/10.1021/acs.chemmater.2c01102.

Detailed description of the experimental methods and used materials; additional QCM measurements; scheme of the growth of Cu-BDC SURMOF by sALD sALD setup; ; and additional characterization data of Cu-BDC (PDF)

AUTHOR INFORMATION

Corresponding Authors

Maïssa K. S. Barr − *Friedrich-Alexander-Universität Erlangen-Nürnberg, Chair Chemistry of Thin Film Materials, IZNF, 91058 Erlangen, Germany;* orcid.org/0000-0003-1587-2269; Email: maissa.barr@fau.de

Engelbert Redel − *Karlsruhe Institute of Technology, Institute of Functional Interfaces (IFG), 76344 Eggenstein-Leopoldshafen, Germany*; Email: engelbert.redel@partner.kit.edu

Authors

Soheila Nadiri − *Friedrich-Alexander-Universität Erlangen-Nürnberg, Chair Chemistry of Thin Film Materials, IZNF, 91058 Erlangen, Germany*

Dong-Hui Chen − *Karlsruhe Institute of Technology, Institute of Functional Interfaces (IFG), 76344 Eggenstein-Leopoldshafen, Germany;* orcid.org/0000-0003-2561-2444

Peter G. Weidler − *Karlsruhe Institute of Technology, Institute of Functional Interfaces (IFG), 76344 Eggenstein-Leopoldshafen, Germany*

Sebastian Bochmann − *Friedrich-Alexander-Universität Erlangen-Nürnberg, Chair Chemistry of Thin Film Materials, IZNF, 91058 Erlangen, Germany*

Helmut Baumgart − *Department of Electrical and Computer Engineering, Old Dominion University, Norfolk, Virginia 23529, United States; Applied Research Center at Jefferson Labs, Newport News, Virginia 23606, United States*

Julien Bachmann − *Friedrich-Alexander-Universität Erlangen-Nürnberg, Chair Chemistry of Thin Film Materials, IZNF, 91058 Erlangen, Germany;* orcid.org/0000-0001-6480-6212

Complete contact information is available at: https://pubs.acs.org/10.1021/acs.chemmater.2c01102

Author Contributions

H.B., E.R., and J.B. initiated the project with the first concept ideas of SURMOF sALD. S.N. performed the deposition and SE characterization; D. C performed the Raman and PM-IRRAS characterizations; P.G.W. performed the XRD measurements; S.B. performed the SEM analysis; M. K.S.B. performed the AFM measurements and the analysis of the data; and M.K.S.B., H.B., E.R., and J.B. wrote the manuscript.

Notes

The authors declare no competing financial interest.

https://doi.org/10.1021/acs.chemmater.2c01102
Chem. Mater. 2022, 34, 9836−9843

■ ACKNOWLEDGMENTS

Financial support was provided by the Deutsche Forschungsgemeinschaft (DFG) within the COORNET Priority Program (SPP 1928), the European Research Council (ERC) in the ERC Consolidator Grant 'Solacylin' (grant agreement 647281), and by FAU via the excellence cluster "Engineering of Advanced Materials" and the "Emerging Talents Initiative". E.R. thanks KIT for sustainable research funding. D.C. acknowledges the financial support of the Chinese Scholarship Council (CSC). Further support from the KNMF (Karlsruhe Nano Micro Facility) is gratefully acknowledged. The authors are thankful to Ryan W. Crisp for proofreading.

■ REFERENCES

(1) James, S. L. Metal-organic frameworks. *Chem. Soc. Rev.* **2003**, *32*, 276−288.
(2) Li, H.; Eddaoudi, M.; O'Keeffe, M.; Yaghi, O. M. Design and synthesis of an exceptionally stable and highly porous metal-organic framework. *Nature* **1999**, *402*, 276−279.
(3) Rowsell, J. L. C.; Yaghi, O. M. Metal-organic frameworks: a new class of porous materials. *Microporous Mesoporous Mater.* **2004**, *73*, 3−14.
(4) Lee, J.; Farha, O. K.; Roberts, J.; Scheidt, K. A.; Nguyen, S. T.; Hupp, J. T. Metal-organic framework materials as catalysts. *Chem. Soc. Rev.* **2009**, *38*, 1450−1459.
(5) Babaei, H., DeCoster, M. E., Jeong, M., Hassan, Z. M., Islamoglu, T., Baumgart, H., McGaughey, A. J. H., Redel, E., Farha, O. K., Hopkins, P. E., Malen, J. A., Wilmer, C. E. Observation of reduced thermal conductivity in a metal-organic framework due to the presence of adsorbates. *Nat. Commun.* **2020**, *11*(). DOI: 10.1038/s41467-020-17822-0
(6) Murray, L. J.; Dincă, M.; Long, J. R. Hydrogen storage in metal-organic frameworks. *Chem. Soc. Rev.* **2009**, *38*, 1294−1314.
(7) Li, J. R.; Sculley, J.; Zhou, H. C. Metal-Organic Frameworks for Separations. *Chem. Rev.* **2012**, *112*, 869−932.
(8) Chen, X.; Wang, Z.; Lin, P.; Zhang, K.; Baumgart, H.; Redel, E.; Wöll, C. Thermoelectric Properties of Highly Ordered Metal-Organic Framework Films. *ECS Trans.* **2016**, *75*, 119−126.
(9) Chen, X.; Wang, Z. B.; Hassan, Z. M.; Lin, P. T.; Zhang, K.; Baumgart, H.; Redel, E. Seebeck Coefficient Measurements of Polycrystalline and Highly Ordered Metal-Organic Framework Thin Films. *ECS J. Solid State Sci. Technol.* **2017**, *6*, P150−P153.
(10) Redel, E.; Baumgart, H. Thermoelectric porous MOF based hybrid materials. *APL Mater.* **2020**, *8*, 060902.
(11) Kreno, L. E.; Leong, K.; Farha, O. K.; Allendorf, M.; Van Duyne, R. P.; Hupp, J. T. Metal-Organic Framework Materials as Chemical Sensors. *Chem. Rev.* **2012**, *112*, 1105−1125.
(12) Bloch, E. D.; Murray, L. J.; Queen, W. L.; Chavan, S.; Maximoff, S. N.; Bigi, J. P.; Krishna, R.; Peterson, V. K.; Grandjean, F.; Long, G. J.; Smit, B.; Bordiga, S.; Brown, C. M.; Long, J. R. Selective Binding of O-2 over N-2 in a Redox-Active Metal-Organic Framework with Open Iron(II) Coordination Sites. *J. Am. Chem. Soc.* **2011**, *133*, 14814−14822.
(13) Bloch, E. D.; Queen, W. L.; Krishna, R.; Zadrozny, J. M.; Brown, C. M.; Long, J. R. Hydrocarbon Separations in a Metal-Organic Framework with Open Iron(II) Coordination Sites. *Science* **2012**, *335*, 1606−1610.
(14) Borfecchia, E.; Maurelli, S.; Gianolio, D.; Groppo, E.; Chiesa, M.; Bonino, F.; Lamberti, C. Insights into Adsorption of NH_3 on HKUST-1 Metal−Organic Framework: A Multitechnique Approach. *J. Phys. Chem. C* **2012**, *116*, 19839−19850.
(15) Kim, H. K.; Yun, W. S.; Kim, M.-B.; Kim, J. Y.; Bae, Y.-S.; Lee, J.; Jeong, N. C. A Chemical Route to Activation of Open Metal Sites in the Copper-Based Metal−Organic Framework Materials HKUST-1 and Cu-MOF-2. *J. Am. Chem. Soc.* **2015**, *137*, 10009−10015.
(16) Clark, R.; Tapily, K.; Yu, K. H.; Hakamata, T.; Consiglio, S.; O'Meara, D.; Wajda, C.; Smith, J.; Leusink, G. Perspective: New process technologies required for future devices and scaling. *APL Mater.* **2018**, *6*, 058203.
(17) Tapily, K.; Jakes, J.; Stone, D.; Shrestha, P.; Gu, D.; Baumgart, H.; Elmustafa, A. Nanomechanical Properties of High-K Dielectrics Grown by Atomic Layer Deposition. *ECS Trans.* **2019**, *11*, 123−130.
(18) Zhu, X.; Gu, D.; Li, Q.; Ioannou, D. E.; Baumgart, H.; Suehle, J. S.; Richter, C. A. Silicon nanowire NVM with high-k gate dielectric stack. *Microelectron. Eng.* **2009**, *86*, 1957−1960.
(19) Puurunen, R. L. Surface chemistry of atomic layer deposition: A case study for the trimethylaluminum/water process. *J. Appl. Phys.* **2005**, *97*, 1−52.
(20) Sundberg, P.; Karppinen, M. Organic and inorganic−organic thin film structures by molecular layer deposition: A review. *Beilstein J. Nanotechnol.* **2014**, *5*, 1104−1136.
(21) Han, S.; Mullins, C. B. Current Progress and Future Directions in Gas-Phase Metal-Organic Framework Thin-Film Growth. *ChemSusChem* **2020**, *13*, 5433−5442.
(22) Meng, X. An overview of molecular layer deposition for organic and organic−inorganic hybrid materials: mechanisms, growth characteristics, and promising applications. *J. Mater. Chem. A* **2017**, *5*, 18326−18378.
(23) Svärd, L.; Putkonen, M.; Kenttä, E.; Sajavaara, T.; Krahl, F.; Karppinen, M.; Van de Kerckhove, K.; Detavernier, C.; Simell, P. Low-Temperature Molecular Layer Deposition Using Monofunctional Aromatic Precursors and Ozone-Based Ring-Opening Reactions. *Langmuir* **2017**, *33*, 9657−9665.
(24) George, S. M.; Yoon, B.; Dameron, A. A. Surface Chemistry for Molecular Layer Deposition of Organic and Hybrid Organic−Inorganic Polymers. *Acc. Chem. Res.* **2009**, *42*, 498−508.
(25) Sønsteby, H. H.; Yanguas-Gil, A.; Elam, J. W. Consistency and reproducibility in atomic layer deposition. *J. Vac. Sci. Technol., A* **2020**, *38*, 020804.
(26) Stassen, I.; Styles, M.; Grenci, G.; Gorp, V.; Vanderlinden, W.; Feyter, D.; Falcaro, P.; Vos, D. D.; Vereecken, P.; Ameloot, R. Chemical vapour deposition of zeolitic imidazolate framework thin films. *Nat. Mater.* **2016**, *15*, 304−310.
(27) Ahvenniemi, E.; Karppinen, M. Atomic/molecular layer deposition: a direct gas-phase route to crystalline metal−organic framework thin films. *Chem. Commun.* **2016**, *52*, 1139−1142.
(28) Ahvenniemi, E.; Karppinen, M. In Situ Atomic/Molecular Layer-by-Layer Deposition of Inorganic−Organic Coordination Network Thin Films from Gaseous Precursors. *Chem. Mater.* **2016**, *28*, 6260−6265.
(29) Lausund, K. B.; Nilsen, O. All-gas-phase synthesis of UiO-66 through modulated atomic layer deposition. *Nat. Commun.* **2016**, *7*, 13578.
(30) Multia, J.; Karppinen, M. Atomic/Molecular Layer Deposition for Designer's Functional Metal−Organic Materials. *Adv. Mater. Interfaces* **2022**, *9*, 2200210.
(31) Stassen, I.; De Vos, D.; Ameloot, R. Vapor-Phase Deposition and Modification of Metal−Organic Frameworks: State-of-the-Art and Future Directions. *Chem. - Eur. J.* **2016**, *22*, 14452−14460.
(32) Stassin, T.; Rodríguez-Hermida, S.; Schrode, B.; Cruz, A. J.; Carraro, F.; Kravchenko, D.; Creemers, V.; Stassen, I.; Hauffman, T.; De Vos, D.; Falcaro, P.; Resel, R.; Ameloot, R. Vapour-phase deposition of oriented copper dicarboxylate metal−organic framework thin films. *Chem. Commun.* **2019**, *55*, 10056−10059.
(33) Stassin, T.; Stassen, I.; Marreiros, J.; Cruz, A. J.; Verbeke, R.; Tu, M.; Reinsch, H.; Dickmann, M.; Egger, W.; Vankelecom, I. F. J.; De Vos, D. E.; Ameloot, R. Solvent-Free Powder Synthesis and MOF-CVD Thin Films of the Large-Pore Metal−Organic Framework MAF-6. *Chem. Mater.* **2020**, *32*, 1784−1793.
(34) Fichtner, J.; Wu, Y.; Hitzenberger, J.; Drewello, T.; Bachmann, J. Molecular Layer Deposition from Dissolved Precursors. *ECS J. Solid State Sci. Technol.* **2017**, *6*, N171−N175.
(35) Koch, V. M.; Barr, M. K. S.; Büttner, P.; Mínguez-Bacho, I.; Döhler, D.; Winzer, B.; Reinhardt, E.; Segets, D.; Bachmann, J. A solution-based ALD route towards $(CH_3NH_3)(PbI_3)$ perovskite via lead sulfide films. *J. Mater. Chem. A* **2019**, *7*, 25112−25119.

(36) Wu, Y.; Döhler, D.; Barr, M.; Oks, E.; Wolf, M.; Santinacci, L.; Bachmann, J. Atomic Layer Deposition from Dissolved Precursors. *Nano Lett.* **2015**, *15*, 6379−6385.
(37) Liu, J.; Lukose, B.; Shekhah, O.; Arslan, H. K.; Weidler, P.; Gliemann, H.; Bräse, S.; Grosjean, S.; Godt, A.; Feng, X.; Müllen, K.; Magdau, I.-B.; Heine, T.; Wöll, C. A novel series of isoreticular metal organic frameworks: realizing metastable structures by liquid phase epitaxy. *Sci. Rep.* **2012**, *2*, 921.
(38) Shekhah, S.; Wang, H.; Kowarik, S.; Schreiber, F.; Paulus, M.; Tolan, M.; Sternemann, C.; Evers, F.; Evers, D.; Zacher, R. A.; Fischer, C.; Wöll, C. Step-by-step route for the synthesis of metal−organic frameworks. *J. Am. Chem. Soc.* **2007**, *129*, 15118−9.
(39) Arslan, H. K.; Shekhah, O.; Wohlgemuth, J.; Franzreb, M.; Fischer, R. A.; Wöll, C. High-Throughput Fabrication of Uniform and Homogenous MOF Coatings. *Adv. Funct. Mater.* **2011**, *21*, 4228−4231.
(40) Arslan, H. K.; Shekhah, O.; Wieland, D. C. F.; Paulus, M.; Sternemann, C.; Schroer, M. A.; Tiemeyer, S.; Tolan, M.; Fischer, R. A.; Wöll, C. Intercalation in layered metal−organic frameworks: reversible inclusion of an extended π-system. *J. Am. Chem. Soc.* **2011**, *133*, 8158−8161.
(41) Lee, J.-C.; Kim, J.-O.; Lee, H.-J.; Shin, B.; Park, S. Meniscus-Guided Control of Supersaturation for the Crystallization of High Quality Metal Organic Framework Thin Films. *Chem. Mater.* **2019**, *31*, 7377−7385.
(42) Mandemaker, L. D. B.; Filez, M.; Delen, G.; Tan, H.; Zhang, X.; Lohse, D.; Weckhuysen, B. M. Time-Resolved In Situ Liquid-Phase Atomic Force Microscopy and Infrared Nanospectroscopy during the Formation of Metal−Organic Framework Thin Films. *J. Phys. Chem. Lett.* **2018**, *9*, 1838−1844.
(43) Haraguchi, T.; Otsubo, K.; Kitagawa, H. Emergence of Surface- and Interface-Induced Structures and Properties in Metal−Organic Framework Thin Films. *Eur. J. Inorg. Chem.* **2018**, *2018*, 1697−1706.
(44) Redel, E.; Wang, Z.; Walheim, S.; Liu, J.; Gliemann, H.; Wöll, C. On the dielectric and optical properties of surface-anchored metal-organic frameworks: A study on epitaxially grown thin films. *Appl. Phys. Lett.* **2013**, *103*, 1−5.
(45) Puurunen, R. Growth Per Cycle in Atomic Layer Deposition: A Theoretical Model. *Chem. Vap. Deposition* **2003**, *9*, 249−257.
(46) Li, X.; Zhou, H.; Qi, F.; Niu, X.; Xu, X.; Qiu, F.; He, Y.; Pan, J.; NiPan, L. Three hidden talents in one framework: a terephthalic acid-coordinated cupric metal−organic framework with cascade cysteine oxidase- and peroxidase-mimicking activities and stimulus-responsive fluorescence for cysteine sensing. *J. Mater. Chem. B* **2018**, *6*, 6207−6211.
(47) Dai, R.; Zhang, X.; Liu, M.; Wu, Z.; Wang, Z. Porous metal organic framework CuBDC nanosheet incorporated thin-film nanocomposite membrane for high-performance forward osmosis. *J. Membr. Sci.* **2019**, *573*, 46−54.
(48) Elder, A. C.; Aleksandrov, A. B.; Nair, S.; Orlando, T. M. Interactions on External MOF Surfaces: Desorption of Water and Ethanol from CuBDC Nanosheets. *Langmuir* **2017**, *33*, 10153−10160.
(49) Wang, B.; Jin, J.; Ding, B.; Han, X.; Han, A.; Liu, J. General Approach to Metal-Organic Framework Nanosheets With Controllable Thickness by Using Metal Hydroxides as Precursors. *Front. Mater.* **2020**, *7*, 1−7.
(50) Kassem, A. A.; Abdelhamid, H. N.; Fouad, D. M.; Ibrahim, S. A. Metal-organic frameworks (MOFs) and MOFs-derived CuO@C for hydrogen generation from sodium borohydride. *Int. J. Hydrogen Energy* **2019**, *44*, 31230−31238.
(51) Yim, C.; Jeon, S. Direct synthesis of Cu-BDC frameworks on a quartz crystal microresonator and their application to studies of n-hexane adsorption. *RSC Adv.* **2015**, *5*, 67454−67458.
(52) Zhang, F. Y.; Zhang, J. L.; Zhang, B. X.; Zheng, L. R.; Cheng, X. Y.; Wan, Q.; Han, B. X.; Zhang, J. CO_2 controls the oriented growth of metal-organic framework with highly accessible active sites. *Nat. Commun.* **2020**, *11*, 1−8.

https://doi.org/10.1021/acs.chemmater.2c01102
Chem. Mater. 2022, 34, 9836−9843